

# A CONSISTENT FINITE ELEMENT FORMULATION FOR NON-LINEAR DYNAMIC ANALYSIS OF PLANAR BEAM

KUO MO HSIAO, RONG TSER YANG AND AN CHEN LEE

*Department of Mechanical Engineering, National Chiao Tung University, 1001 Tahsueh Road, Hsinchu, Taiwan, Republic of China*

## SUMMARY

A co-rotational finite element formulation for the dynamic analysis of planar Euler beam is presented. Both the internal nodal forces due to deformation and the inertia nodal forces are systematically derived by consistent linearization of the fully geometrically non-linear beam theory using the d'Alembert principle and the virtual work principle. Due to the consideration of the exact kinematics of Euler beam, some velocity coupling terms are obtained in the inertia nodal forces. An incremental-iterative method based on the Newmark direct integration method and the Newton–Raphson method is employed here for the solution of the non-linear dynamic equilibrium equations. Numerical examples are presented to investigate the effect of the velocity coupling terms on the dynamic response of the beam structures.

## 1. INTRODUCTION

In recent years, the non-linear dynamic behaviour of beam structures, e.g. framed structures, flexible mechanisms and robot arms, has been the subject of considerable research.<sup>1–13</sup> Hsiao and Jang<sup>11</sup> presented a co-rotational formulation and numerical procedure for the dynamic analysis of planar beam structures. In this formulation the Euler–Bernoulli hypothesis was employed and the unit extension of the centroid axis of the beam element was assumed to be constant. As extensively used in the literature, the inertia nodal force vector was obtained simply by the inner product of the mass matrix and the nodal acceleration vector. This formulation and numerical procedure were proven to be very effective by numerical examples studied in Reference 11. However, the inertia nodal forces used in Reference 11 are derived from the linear beam theory. As mentioned in Reference 9, the use of linear beam theory cannot account for the complete inertia effects. In order to capture all inertia effects and coupling among extensional, flexural and torsional deformations for beam elements, the formulation of beam elements might be derived from the fully geometrically non-linear beam theory by consistent linearization.<sup>9</sup> Two consistent co-rotational formulations for three-dimensional beam element are proposed by Crisfield<sup>14</sup> and Hsiao,<sup>15</sup> respectively. However, they are only limited for non-linear static analysis.

The objective of this study is to present a consistent formulation for the dynamic analysis of planar Euler beam in which the inertia nodal forces and internal nodal forces due to deformation are systematically derived by consistent linearization of the fully geometrically non-linear beam theory using the d'Alembert principle and the virtual work principle. Here the Euler–Bernoulli hypothesis is properly considered.<sup>16</sup> Following Reference 11, the nodal co-ordinates, incremental displacements and rotations, velocities, accelerations and the equations of motion of the system are defined in terms of a fixed global co-ordinate system, while the total strains in the beam

element are measured in element co-ordinates which are constructed at the current configuration of the beam element. The element equations are constructed first in the element co-ordinate system and then transformed to the global co-ordinate system using standard procedure. The dominant factors in the geometrical non-linearities of beam structures are attributable to finite rotations, the strains remaining small. For a beam structure discretized by finite elements, this implies that the motion of the individual elements to a large extent will consist of rigid-body motion. If the rigid-body motion part is eliminated from the total displacements and the element size is properly chosen, the deformational part of the motion is always small relative to the local element axes; thus, in conjunction with the co-rotational formulation, the higher-order terms of nodal parameters in the element internal nodal forces and inertia nodal forces may be neglected. Due to the consideration of the exact kinematics of Euler beam, some velocity coupling terms are retained in the inertia nodal forces.

An incremental-iterative method based on the Newmark direct integration method and the Newton-Raphson method is employed here for the solution of the non-linear dynamic equilibrium equations. Numerical examples are presented to investigate the effect of the velocity coupling terms on the dynamic response of the beam structures.

## 2. NON-LINEAR FORMULATION

### 2.1. Basic assumptions

The following assumptions are made in derivation of the non-linear behaviour:

- (1) The Euler-Bernoulli hypothesis is valid.
- (2) The unit extension of the centroid axis of the beam element is uniform.
- (3) The deformational displacements and rotations of the beam element are small.
- (4) The strain of the beam element is small.

The third assumption can always be satisfied if the element size is properly chosen. Due to the assumption of small strain, the engineering strain and stress are used for the measure of the strain and stress. For convenience, the engineering strain is obtained from the corresponding Green strain in this study.

### 2.2. Co-ordinate systems

In order to describe the system, following Reference 11, we define two sets of co-ordinate systems (see Figure 1):

- (1) A fixed global set of co-ordinates,  $X_1, X_2$ . The nodal co-ordinates, incremental displacements and rotations, velocities, accelerations, and the equations of motion of the system are defined in this co-ordinate system.
- (2) Element co-ordinates,  $x_1, x_2$ . A set of element co-ordinates associated with each element, which is constructed at the current configuration of the beam element. The element equations are constructed first in the element co-ordinate system and then transformed to the global co-ordinate system using standard procedure.

### 2.3. Nodal parameters and nodal forces

The element employed here has three degrees of freedom per node (Figure 2): these are the translations  $u_j$  and  $v_j$  ( $j = 1, 2$ ) in the  $x_1$  and  $x_2$  directions, respectively, and the counterclockwise

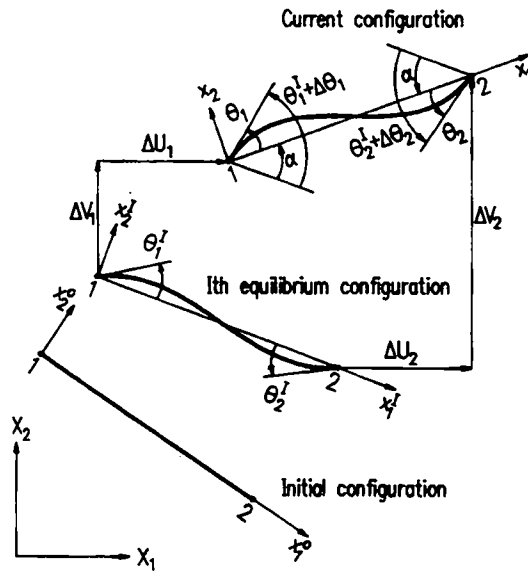


Figure 1. Co-ordinate systems

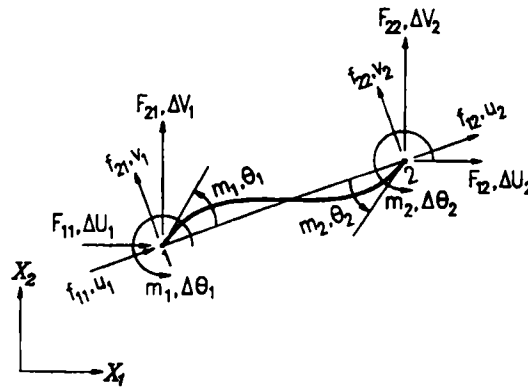


Figure 2. Nodal parameters and nodal forces

rotations  $\theta_j$  ( $j = 1, 2$ ) at nodes  $j$ . The nodal degrees of freedom for the global co-ordinate system are the incremental translations  $\Delta U_j$  and  $\Delta V_j$  ( $j = 1, 2$ ) in the  $X_1$  and  $X_2$  directions, respectively, and the incremental counterclockwise rotations  $\Delta\theta_j$  ( $j = 1, 2$ ) at nodes  $j$ . The nodal forces corresponding to the nodal parameters are the conventional forces and moments as shown in Figure 2.

2.4. Kinematics of beam elements

The geometry of the beam element is described in the element co-ordinate system. In this study, the symbol  $\{ \}$  denotes column matrix. Let  $Q$  (Figure 3) be an arbitrary point in the beam

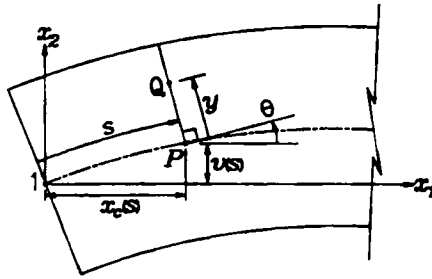


Figure 3. Kinematics of the deformed beam

element, and  $P$  be the corresponding point of  $Q$  on the centroid axis. The position vector of point  $P$  in the undeformed and deformed configurations can be expressed as  $\{x, 0\}$  and  $\{x_c(s), v(s)\}$ , respectively, where  $s$  is the arc length of the deformed centroid axis measured from node 1 to point  $P$ . The relationship among  $x_c(s)$ ,  $v(s)$ , and  $s$  may be given as

$$x_c(s) = u_1 + \frac{S}{2} \int_{-1}^{\xi} \cos \theta d\xi \quad (1)$$

where

$$\cos \theta = (1 - v'^2)^{1/2} \quad (2)$$

$$v' = \frac{dv(s)}{ds} = \sin \theta \quad (3)$$

and

$$\xi = -1 + \frac{2s}{S} \quad (4)$$

in which  $u_1$  is the displacement of node 1 in the  $x_1$  direction,  $\theta$  is the angle measured from the  $x_1$  axis to the tangent of the centroid axis and  $S$  is the current arc length of the centroid axis of the beam element. Note that due to the definition of the element co-ordinate system, the value of  $u_1$  is equal to zero. However, the variation and the time derivative of  $u_1$  are not zero. Making use of equation (1), we obtain

$$S = \frac{2\ell}{\beta} \quad (5)$$

where

$$\beta = \int_{-1}^1 \cos \theta d\xi \quad (6)$$

and

$$\ell = x_c(S) - x_c(0) = L - u_1 + u_2 \quad (7)$$

in which  $L$  is the length of the undeformed beam axis and  $u_2$  is the displacement of node 2 in the  $x_1$  direction.

The position vector of point  $Q$  in the undeformed and deformed configuration may be written as

$$\mathbf{r}_0 = \{x, y\} \quad (8)$$

and

$$\mathbf{r}(s) = \{x_c(s) - y \sin \theta, v(s) + y \cos \theta\} \quad (9)$$

and displacement vector of point  $Q$  may be given by

$$\mathbf{u} = \mathbf{r} - \mathbf{r}_0 \quad (10)$$

If  $x$  and  $y$  are regarded as the independent variables, the Green strains  $\varepsilon_{ij}$  ( $i = 1, 2, j = 1, 2$ ) are given by<sup>17</sup>

$$\varepsilon_{ij} = \frac{1}{2}(\mathbf{G}_i^T \mathbf{G}_j - \mathbf{g}_i^T \mathbf{g}_j) \quad (11)$$

where

$$\begin{aligned} \mathbf{G}_1 &= \frac{\partial \mathbf{r}}{\partial x} = \frac{\partial \mathbf{r}}{\partial s} \frac{\partial s}{\partial x} = (1 + \varepsilon_0)(1 - \kappa y) \{\cos \theta, \sin \theta\} \\ \mathbf{G}_2 &= \frac{\partial \mathbf{r}}{\partial y} = \{-\sin \theta, \cos \theta\} \\ \mathbf{g}_1 &= \frac{\partial \mathbf{r}_0}{\partial x} = \{1, 0\} \\ \mathbf{g}_2 &= \frac{\partial \mathbf{r}_0}{\partial y} = \{0, 1\} \end{aligned} \quad (12)$$

$$\varepsilon_0 = \frac{\partial s}{\partial x} - 1 \quad (13)$$

and

$$\kappa = \frac{\partial \theta}{\partial s} = cv'' \quad (14)$$

in which

$$c = 1/\cos \theta \quad (15)$$

$$v'' = \frac{d^2 v}{ds^2} \quad (16)$$

Note that  $\kappa$  in equation (14) is an exact expression for the physical curvature of the deformed beam centroid axis. An equivalent expression of  $\kappa$  is given in Reference 16. Making use of the assumption of uniform unit extension, we may rewrite the unit extension  $\varepsilon_0$  in equation (13) as

$$\varepsilon_0 = \frac{S}{L} - 1 \quad (17)$$

Due to the use of the Euler–Bernoulli hypothesis, as expected,  $\varepsilon_{11}$  is the only non-zero component of  $\varepsilon_{ij}$ . Substituting equation (12) into equation (11) we may obtain

$$\varepsilon_{11} = \frac{1}{2}[(1 + \varepsilon_0)^2(1 - \kappa y)^2 - 1] \quad (18)$$

The engineering strain corresponding to  $\varepsilon_{11}$  is given by<sup>17</sup>

$$\varepsilon = (1 + 2\varepsilon_{11})^{1/2} - 1 = (1 + \varepsilon_0)(1 - \kappa y) - 1 \quad (19)$$

Note that  $\varepsilon$  in equation (19) is an exact expression of engineering strain for the Euler beam.

Here, the lateral displacement of the centroid axis,  $v(s)$  is assumed to be the cubic Hermitian polynomials of  $s$  and is given by

$$v(s) = \{N_1, N_2, N_3, N_4\}^T \{v_1, v'_1, v_2, v'_2\} = \mathbf{N}_b^T \mathbf{u}_b, \quad (20)$$

where  $v_j$  and  $v'_j$  ( $j = 1, 2$ ) are the nodal value of  $v$  and  $v'$  at nodes  $j$ , respectively.  $N_i$  ( $i = 1-4$ ) are shape functions and are given by

$$\begin{aligned} N_1 &= \frac{1}{4}(1 - \xi)^2(2 + \xi), & N_2 &= \frac{1}{8}S(1 - \xi^2)(1 - \xi) \\ N_3 &= \frac{1}{4}(1 + \xi)^2(2 - \xi), & N_4 &= \frac{1}{8}S(-1 + \xi^2)(1 + \xi) \end{aligned} \quad (21)$$

where  $S$  is the current arc length of the centroid axis, and  $\xi$  is the non-dimensional co-ordinate defined in equation (4).

### 2.5. Element internal nodal force vectors

The element internal nodal forces are obtained from the d'Alembert principle and the virtual work principle. The virtual work principle requires that

$$\delta \mathbf{u}_a^T \mathbf{f}_a + \delta \mathbf{u}_b^T \mathbf{f}_b = \int_V (\delta \varepsilon^T \sigma + \rho \delta \mathbf{u}^T \ddot{\mathbf{u}}) dV \quad (22)$$

where

$$\delta \mathbf{u}_a = \{\delta u_1, \delta u_2\} \quad (23)$$

$$\delta \mathbf{u}_b = \{\delta v, \delta \theta_1, \delta v_2, \delta \theta_2\} \quad (24)$$

$$\mathbf{f}_a = \mathbf{f}_a^d + \mathbf{f}_a^i = \{f_{11}, f_{12}\} \quad (25)$$

$$\mathbf{f}_b = \mathbf{f}_b^d + \mathbf{f}_b^i = \{f_{21}, m_1, f_{22}, m_2\} \quad (26)$$

in which  $\mathbf{f}_j^d$  and  $\mathbf{f}_j^i$  ( $j = a, b$ ) are the nodal force vector due to deformations and the inertia nodal force vector, respectively.  $\delta \varepsilon$  is the variation of  $\varepsilon$  given in equation (19).  $\sigma = E\varepsilon$  is the normal stress, where  $E$  is the Young's modulus.  $\rho$  is the density,  $\delta \mathbf{u}$  is the variation of  $\mathbf{u}$  given in equation (10) with respect to the nodal parameters, and  $\ddot{\mathbf{u}} = d^2 \mathbf{u} / dt^2$ . In this paper, the symbol ( $\dot{\phantom{x}}$ ) denotes differentiation with respect to time  $t$ ,  $V$  is the volume of the undeformed beam.

The exact expression of  $\mathbf{f}_a$  and  $\mathbf{f}_b$  may be obtained by substituting the exact expression of  $\delta \varepsilon$ ,  $\varepsilon$ ,  $\delta \mathbf{u}$ , and  $\ddot{\mathbf{u}}$  into equation (22). However, if the element size is properly chosen, the nodal parameters of the element may always be much smaller than unity. Thus, only the first-order terms of nodal parameters are retained in  $\mathbf{f}_a^d$  and  $\mathbf{f}_b^d$ , and only zeroth-order terms of nodal parameters are retained in  $\mathbf{f}_a^i$  and  $\mathbf{f}_b^i$ . However, in order to include the effect of axial force, a second-order term of nodal parameters is retained in  $\mathbf{f}_b^d$ . The approximations,  $1 + \varepsilon_0 \approx 1$ ,  $v' \approx \theta$  and  $\cos \theta \approx 1$  are used in the derivation of  $\mathbf{f}_a$  and  $\mathbf{f}_b$ . In order to avoid improper omission in the derivation of  $\mathbf{f}_a$  and  $\mathbf{f}_b$ , these approximations are applied to the exact expression of  $\delta \varepsilon$ ,  $\varepsilon$ ,  $\delta \mathbf{u}$  and  $\ddot{\mathbf{u}}$ .

From equations (2)–(7) and (14)–(17), the variation of  $\varepsilon$  in equation (19) may be expressed as

$$\delta \varepsilon = (1 - \kappa y) \delta \varepsilon_0 - (1 + \varepsilon_0) y \delta \kappa \quad (27)$$

where

$$\delta \kappa = c \delta v'' + c^3 v' v'' \delta v' \quad (28)$$

$$\delta \varepsilon_0 = \frac{\delta S}{L} = \frac{2\delta \ell}{\beta L} - \frac{2\ell \delta \beta}{\beta^2 L} \quad (29)$$

$$\delta\ell = \{-1, 1\}^T \{\delta u_1, \delta u_2\} = \mathbf{G}_a^T \delta \mathbf{u}_a \quad (30)$$

$$\delta\beta = - \int_{-1}^1 cv' \delta v' d\xi \quad (31)$$

in which  $\delta v'$  and  $\delta v''$  are the variations of  $v'$  and  $v''$ , respectively, with respect to the nodal parameters. It should be noted that because the shape functions of  $v'$  and  $v''$  are functions of  $S$ , the current arc length of the centroid axis, the variation of the shape functions are considered here.

From equations (20), (21) and (28)–(31), the exact expression of  $\delta\varepsilon$  in equation (27) may be obtained. Using the approximations  $1 + \varepsilon_0 \approx 1$ ,  $v' \approx \theta$  and  $\cos \theta \approx 1$ , and retaining all zeroth-order terms and one first-order term of nodal parameters in the exact expression of  $\delta\varepsilon$ , we may obtain

$$\delta\varepsilon = \frac{1}{L} \mathbf{G}_a^T \delta \mathbf{u}_a + \frac{1}{2} \int_{-1}^1 v' \mathbf{N}_b'^T d\xi \delta \mathbf{u}_b^e - y \mathbf{N}_b''^T \delta \mathbf{u}_b^e \quad (32)$$

From equations (1)–(9), (20) and (21), the exact expression for  $\delta \mathbf{u}$ , the variation of  $\mathbf{u}$  in equation (10) may be obtained. Using the approximations  $1 + \varepsilon_0 \approx 1$ ,  $v' \approx \theta$  and  $\cos \theta \approx 1$ , and retaining all zeroth-order terms of nodal parameters in the exact expression of  $\delta \mathbf{u}$ , we may obtain

$$\delta \mathbf{u} = \{\mathbf{N}_a^T \delta \mathbf{u}_a - y \mathbf{N}_b'^T \delta \mathbf{u}_b^e, \mathbf{N}_b^T \delta \mathbf{u}_b^e\} \quad (33)$$

where

$$\mathbf{N}_a = \left\{ \frac{1 - \xi}{2}, \frac{1 + \xi}{2} \right\} \quad (34)$$

From equations (1)–(10), (20) and (21), the exact expression of  $\ddot{\mathbf{u}}$  may be obtained. Using the approximations  $1 + \varepsilon_0 \approx 1$ ,  $v' \approx \theta$  and  $\cos \theta \approx 1$ , and retaining only zeroth-order terms of nodal parameters in the exact expression of  $\ddot{\mathbf{u}}$ , we may obtain

$$\begin{aligned} \ddot{\mathbf{u}} = & \left\{ \mathbf{N}_a^T \ddot{\mathbf{u}}_a + \frac{L(1 + \xi)}{4} \int_{-1}^1 (\mathbf{N}_b'^T \ddot{\mathbf{u}}_b)^2 d\xi - \frac{L}{2} \int_{-1}^{\xi} (\mathbf{N}_b'^T \ddot{\mathbf{u}}_b)^2 d\xi \right. \\ & \left. + \frac{2y}{L} \mathbf{N}_c^T \ddot{\mathbf{u}}_b \mathbf{G}_a^T \ddot{\mathbf{u}}_a - y \mathbf{N}_b'^T \ddot{\mathbf{u}}_b, \mathbf{N}_b^T \ddot{\mathbf{u}}_b - y (\mathbf{N}_b'^T \ddot{\mathbf{u}}_b)^2 + \frac{2}{L} \mathbf{G}_a^T \ddot{\mathbf{u}}_a \mathbf{N}_c^T \ddot{\mathbf{u}}_b \right\} \quad (35) \end{aligned}$$

where

$$\dot{\mathbf{u}}_a = \{\dot{u}_1, \dot{u}_2\}, \quad \ddot{\mathbf{u}}_a = \{\ddot{u}_1, \ddot{u}_2\} \quad (36)$$

$$\dot{\mathbf{u}}_b = \{\dot{v}_1, \dot{\theta}_1, \dot{v}_2, \dot{\theta}_2\}, \quad \ddot{\mathbf{u}}_b = \{\ddot{v}_1, \ddot{\theta}_1, \ddot{v}_2, \ddot{\theta}_2\} \quad (37)$$

and

$$\mathbf{N}_c = \{N'_1, 0, N'_3, 0\}, \quad \mathbf{N}_e = \{0, N_2, 0, N_4\} \quad (38)$$

Note that  $\dot{\mathbf{u}}_i$  and  $\ddot{\mathbf{u}}_i$  ( $i = a, b$ ) are the absolute velocity and acceleration vectors of an element referred to the element co-ordinates which are obtained from the transformation of the corresponding global velocity and acceleration vectors extracted from the equations of motion of the system using standard procedure.<sup>11</sup>

Substituting equations (19), (32), (33) and (35) into equation (22), using the approximations  $1 + \varepsilon_0 \approx 1$ ,  $v' \approx \theta$  and  $\cos \theta \approx 1$ , dropping higher-order terms of nodal parameters, and equating the terms on both sides of equation (22) corresponding to virtual displacement vectors  $\delta \mathbf{u}_a$  and

$\delta \mathbf{u}_b^e$ , respectively, we may obtain

$$\mathbf{f}_a^d = AE\varepsilon_0 \mathbf{G}_a \quad (39)$$

$$\mathbf{f}_b^d = \frac{AE\varepsilon_0 L}{2} \int_{-1}^1 \mathbf{N}_b' \mathbf{N}_b'^T d\xi \mathbf{u}_b + \frac{EIL}{2} \int_{-1}^1 \mathbf{N}_b'' \mathbf{N}_b''^T d\xi \mathbf{u}_b \quad (40)$$

$$\begin{aligned} \mathbf{f}_a^i = & \frac{\rho AL}{2} \int_{-1}^1 \mathbf{N}_a \mathbf{N}_a^T d\xi \ddot{\mathbf{u}} \\ & + \frac{\rho AL}{2} \int_{-1}^1 \mathbf{N}_a \left[ \frac{L(1+\xi)}{4} \int_{-1}^1 (\mathbf{N}_b'^T \dot{\mathbf{u}}_b)^2 d\xi - \frac{L}{2} \int_{-1}^{\xi} (\mathbf{N}_b'^T \dot{\mathbf{u}}_b)^2 d\xi \right] d\xi \end{aligned} \quad (41)$$

$$\begin{aligned} \mathbf{f}_b^i = & \frac{\rho AL}{2} \int_{-1}^1 \mathbf{N}_b \mathbf{N}_b^T d\xi \ddot{\mathbf{u}}_b + \frac{\rho IL}{2} \int_{-1}^1 \mathbf{N}_b' \mathbf{N}_b'^T d\xi \ddot{\mathbf{u}}_b \\ & + \frac{\rho A \mathbf{G}_a^T \dot{\mathbf{u}}_a}{2} \int_{-1}^1 \mathbf{N}_b \mathbf{N}_b^T d\xi \dot{\mathbf{u}}_b - \frac{\rho I \mathbf{G}_a^T \dot{\mathbf{u}}_a}{2} \int_{-1}^1 \mathbf{N}_b' \mathbf{N}_b'^T d\xi \dot{\mathbf{u}}_b \end{aligned} \quad (42)$$

where  $A$  is the cross-sectional area and  $I = \int_A y^2 dA$ . The underlined terms in equations (41) and (42) are called the velocity coupling terms in this study. Note that if the velocity coupling terms in equations (41) and (42) are dropped, equations (39)–(42) are identical to the element nodal forces in Reference 11.

## 2.6. Element matrices

The element stiffness matrices and mass matrices may be obtained by differentiating the element nodal force vectors in equations (39)–(42) with respect to nodal parameters, and time derivatives of nodal parameters. However, element matrices are only used to obtain predictors and correctors for incremental solutions of non-linear equations in this study. Approximate element matrices can meet these requirements. Thus, the element matrices used in Reference 11 are adopted here for simplicity.

## 2.7. Equations of motion

The non-linear equations of motion may be expressed by

$$\boldsymbol{\Phi} = \mathbf{F}^I + \mathbf{F}^D - \mathbf{P} = \mathbf{0} \quad (43)$$

where  $\boldsymbol{\Phi}$  is the unbalanced force among the inertia force  $\mathbf{F}^I$ , internal nodal force due to deformation  $\mathbf{F}^D$ , and the external nodal force  $\mathbf{P}$ .  $\mathbf{F}^I$  and  $\mathbf{F}^D$  are assembled from the element nodal force vectors in equations (39)–(42), which must be transformed from element co-ordinate system to global co-ordinate system before assemblage using standard procedure.

In this paper, an weighted Euclidean norm of the unbalanced force is employed for the equilibrium iterations, and is given by

$$e = \frac{\|\boldsymbol{\Phi}\|}{N \|\boldsymbol{\Phi}_r\|} \leq e_{tol} \quad (44)$$

where  $\boldsymbol{\Phi}_r$  is a reference unbalanced force, which is chosen to be the unbalanced force obtained at the first iteration in the present study;  $e_{tol}$  is a prescribed value of error tolerance.



3. APPLICATIONS

An incremental iterative method based on the Newmark direct integration method<sup>11,18</sup> and the Newton-Raphson method is employed. The procedure used here to determine the deformational nodal rotations for individual elements is the same as that proposed in Reference 11 and is not repeated here.

In order to investigate the effect of the velocity coupling terms on the dynamic response, four examples are studied for the cases with and without consideration of the velocity coupling terms. It is found that for the first three examples the results obtained for both cases are nearly identical, but for the last example the discrepancies between the results obtained for both cases are not negligible.

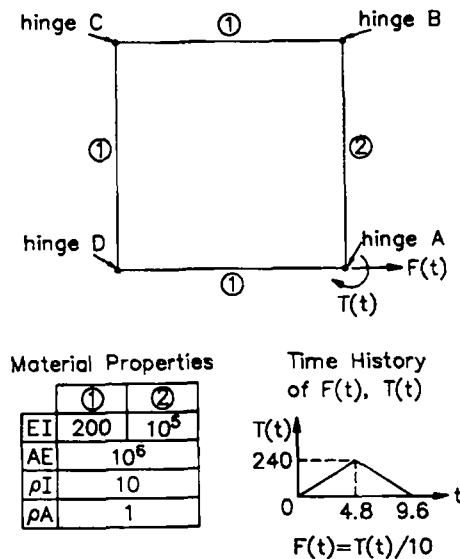


Figure 4. Flying closed-loop chain

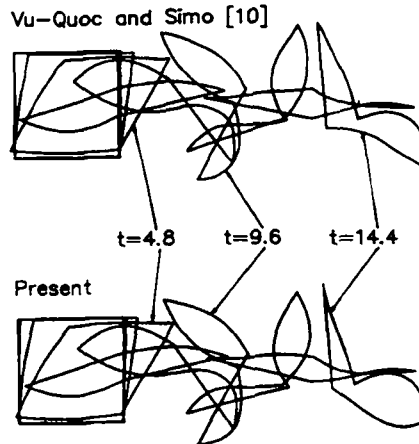


Figure 5. Entire sequence of motion for flying closed-loop chain

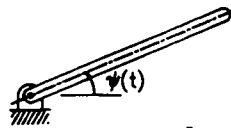
### 3.1. Flying closed-loop chain

The first example considered is a closed-loop chain<sup>10</sup> constituted of four flexible links interconnected by hinges as shown in Figure 4. The geometry and material properties of the closed-loop chain are also shown in Figure 4. Initially, the closed-loop chain forms a square of length 10 on each side. The whole system has no prescribed displacement boundary condition. A force and torque are applied at end A of the link AB as shown in Figure 4. The closed-loop chain is discretized using 40 equal elements. The time step size is set to 0.01 and the error tolerance is set to  $10^{-7}$ . The entire sequence of motion is shown in Figure 5. Also shown in Figure 5 are the results reported in Reference 10. It is observed that the present results are in agreement with those in Reference 10.

### 3.2. Flexible robot arm with end rotation

This example considered is a flexible beam rotating horizontally about a vertical axis passing through one end.<sup>6</sup> Figure 6(a) shows the geometry of the beam and material properties. This beam is subjected to a prescribed rotation angle  $\psi(t)$  at one end as follows:

$$\psi(t) = \begin{cases} \frac{6}{15} \left[ \frac{t^2}{2} + \left( \frac{15}{2\pi} \right)^2 \left( \cos \frac{2\pi t}{15} - 1 \right) \right] \text{rad}, & 0 \leq t \leq 15 \\ (6t - 45) \text{rad}, & t > 15 \end{cases}$$



$$\begin{aligned} AE &= 2.8 \times 10^7 \\ EI &= 1.4 \times 10^4 \\ \rho A &= 1.2 \\ \rho I &= 6 \times 10^{-4} \\ L &= 10 \end{aligned}$$

Figure 6(a). Flexible robot arm

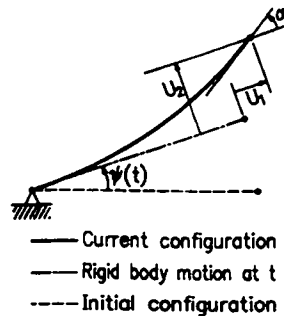


Figure 6(b). Definition of  $U_1$ ,  $U_2$  and  $\alpha$

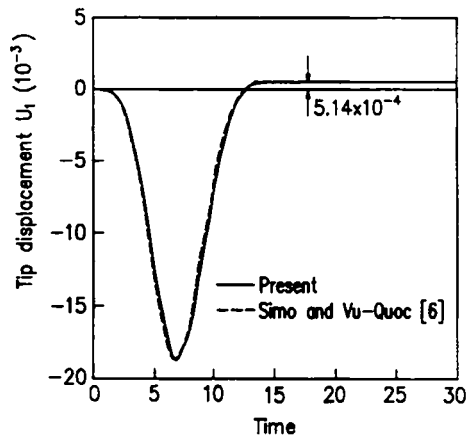


Figure 7(a). Time history for displacement component  $U_1$

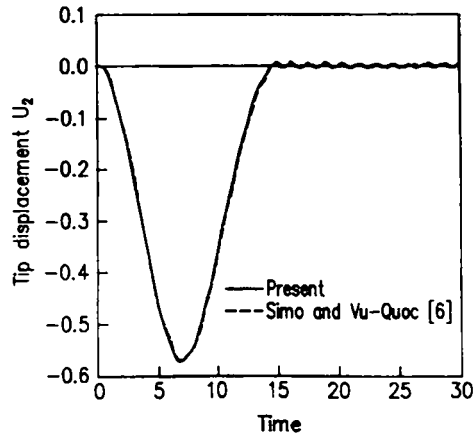


Figure 7(b). Time history for displacement component  $U_2$

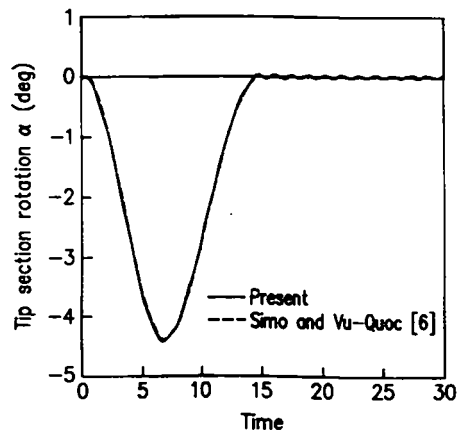


Figure 7(c). Time history for displacement component  $\alpha$

The beam is discretized using four elements. The time step size is set to 0.005 and the error tolerance is set to  $10^{-10}$ . The time histories of the tip displacements  $U_1$ ,  $U_2$ , and the tip rotation  $\alpha$ , which are defined in Figure 7(b), are shown in Figures 7(a)–(c). Also shown in Figures 7(a)–(c) are the results reported in Reference 6. It is observed that the present results are in agreement with those in Reference 6.

3.3. Planar manipulator

The planar manipulator<sup>8</sup> shown in Figure 8 consists of two links. Two cases are considered: (a) both links are considered flexible and (b) link 1 is considered rigid. The geometry, inertia properties and material properties of the planar manipulator are given in Figure 8. For case (b), the Young's modulus of link 1 is set to  $10^4$  times as large as that of link 2 to simulate rigid link. Link 1 rotates with constant angular velocity  $\omega = 10$  rad/s, while the motion of link 2 is such that its tangent at point A always remains in the horizontal position. This is assumed to be achieved by the joint moment. Weight of the bodies acts in the downward direction.

Initially,  $\theta_1 = \theta_2 = 0$ . The initial elastic deformations are assumed to be zero, and the initial velocities and accelerations of the manipulator are calculated by using kinematics of rigid mechanism. Each member is discretized by four elements. The time step size is chosen to be 0.0013 s and the error tolerance is set to  $10^{-12}$ .

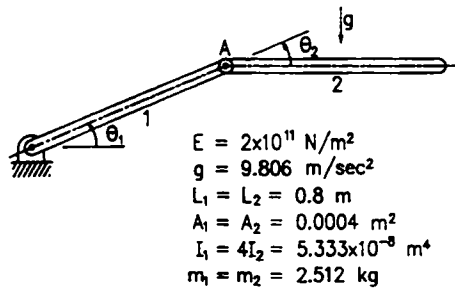


Figure 8. Planar manipulator

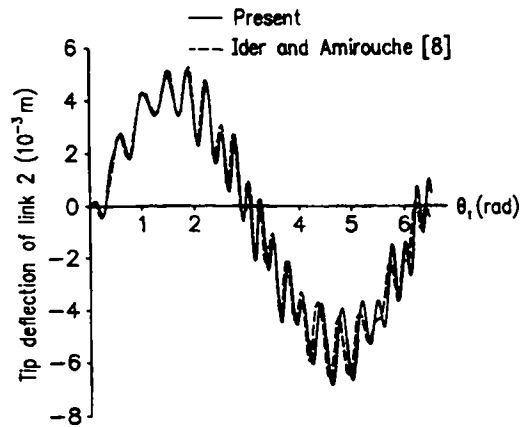


Figure 9(a). Tip deflection of link 2 (both links flexible)

The transverse tip deflections of link 2 measured from the tangent at point A are shown in Figures 9(a) and 9(b) for both cases. Also shown in these figures are the results reported in Reference 8. It is seen that the agreement between these two solutions is very good.

3.4. Flexible robot arm with end torque

The flexible beam as shown in Figure 10 is subjected to an end torque. Initially,  $\psi = 0$ . The beam is discretized by ten elements. The time step size is chosen to be 0.0002 s and the error tolerance is set to  $10^{-10}$ .

The sequence of motion is depicted in Figure 11, and the time history of the rotation angle of the tangent at the robot base is shown in Figure 12. It is observed that the discrepancies between the results for the cases with and without the consideration of the velocity coupling terms are remarked.

4. CONCLUSIONS

This paper has described a consistent finite element formulation for the dynamic analysis of planar Euler beam in which the inertia nodal forces and internal nodal forces due to deformation are systematically derived by consistent linearization of the fully geometrically non-linear beam

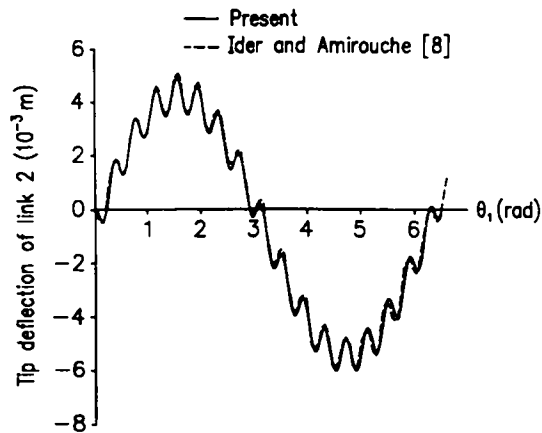


Figure 9(b). Tip deflection of link 2 (link 1 rigid)

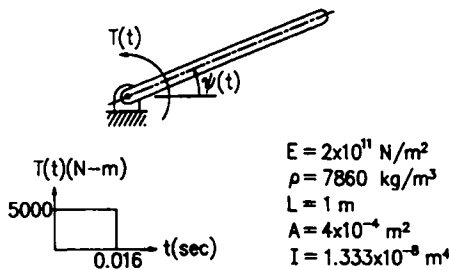


Figure 10. Flexible robot arm with end torque

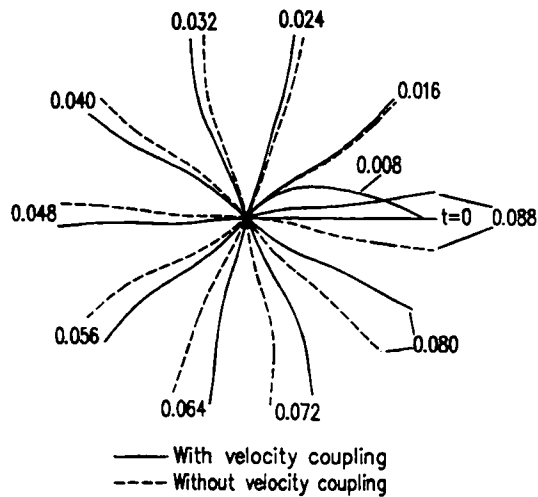


Figure 11. Sequence of motion for flexible robot arm

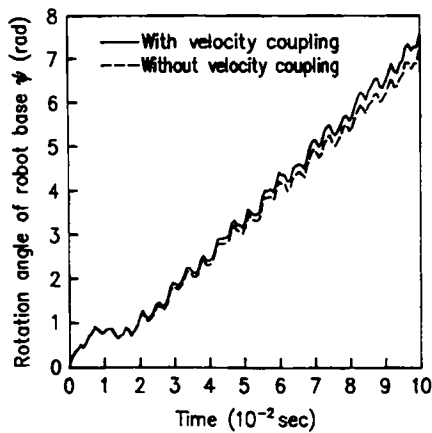


Figure 12. Time history for rotation angle of the tangent at robot base

theory using the d'Alembert principle and the virtual work principle. In conjunction with the co-rotational formulation, the higher-order terms of nodal parameters in element nodal forces are consistently neglected. Due to the consideration of the exact kinematics of the Euler beam, some velocity coupling terms are obtained in the inertia nodal forces. From the numerical examples studied, it is found that the effects of these velocity coupling terms on the dynamic response are remarked for some cases.

Although not included in the present derivation, the inclusion of damping forces presents no difficulties. It is believed that the consistent co-rotational formulation for beam element presented here may represent a valuable engineering tool for the dynamic analysis of planar beam structures.

## ACKNOWLEDGEMENT

The authors would like to acknowledge the constructive and thoughtful comments of the referees. The research was sponsored by the National Science Council, Republic of China, under the contract NSC79-0401-e009-15.

## REFERENCES

1. K.-J. Bathe and E. Ramm, 'Finite element formulations for large deformation dynamic analysis', *Int. j. numer. methods eng.*, **9**, 353–386 (1975).
2. C. Oran and K. Kassimali, 'Large deformations of framed structures under static and dynamic loads', *Comput. Struct.*, **6**, 539–547 (1976).
3. D. P. Mondkar and G. H. Powell, 'Finite element analysis of non-linear static and dynamic response', *Int. j. numer. methods eng.*, **11**, 499–520 (1977).
4. S. N. Remseth, 'Nonlinear static and dynamic analysis of framed structures', *Comput. Struct.*, **10**, 879–897 (1979).
5. T. Y. Yang and S. Saigal, 'A simple element for static and dynamic response of beams with material and geometric nonlinearities', *Int. j. numer. methods eng.*, **20**, 851–867 (1984).
6. J. C. Simo and L. Vu-Quoc, 'On the dynamics of flexible beams under large overall motions—the planar case: Part I and Part II', *J. Appl. Mech. ASME*, **53**, 849–863 (1986).
7. T. R. Kane, R. R. Ryan and A. K. Banerjee, 'Dynamics of a cantilever beam attached to a moving base', *J. Guidance Control Dyn.*, **10**, 139–151 (1987).
8. S. K. Ider and F. M. L. Amirouche, 'Nonlinear modeling of flexible multibody systems dynamics subjected to variable constraints', *J. Appl. Mech. ASME*, **56**, 444–450 (1989).
9. J. C. Simo and L. Vu-Quoc, 'The role of non-linear theories in transient dynamic analysis of flexible structures', *J. Sound Vib.*, **119**, 487–508 (1987).
10. L. Vu-Quoc and J. C. Simo, 'Dynamics of earth-orbiting flexible satellites with multibody components', *J. Guidance Control Dyn.*, **10**, 549–558 (1987).
11. K. M. Hsiao and J. Y. Jang, 'Nonlinear dynamic analysis of elastic frames', *Comput. Struct.*, **33**, 1057–1063 (1989).
12. Z. Yang and J. P. Sadler, 'Large-displacement finite element analysis of flexible linkages', *J. Mech. Design ASME*, **112**, 175–182 (1990).
13. A. K. Banerjee and M. E. Lemak, 'Multi-flexible body dynamics capturing motion-induced stiffness', *J. Appl. Mech. ASME*, **58**, 766–775 (1991).
14. M. A. Crisfield, 'A consistent co-rotational formulation for non-linear, three-dimensional, beam-elements', *Comput. Methods Appl. Mech. Eng.*, **81**, 131–150 (1990).
15. K. M. Hsiao, 'Cororational total Lagrangian formulation for three-dimensional beam element', *AIAA J.*, **30**, 797–804 (1992).
16. D. H. Hodges, 'Proper definition of curvature in nonlinear beam kinematics', *AIAA J.*, **22**, 1825–1827 (1983).
17. T. J. Chung, *Continuum Mechanics*, Prentice-Hall, Englewood Cliffs, N.J., 1988.
18. K. J. Bathe, *Finite Element Procedures in Engineering Analysis*, Prentice-Hall, Englewood Cliffs, N.J., 1982.